Sensor phenomena

Common Mode Current Effect Reduction Method for NEMP Current Sensors Calibration Techniques

Damien Gapillout and Pierre Pradel
CEA Gramat, 46500 Gramat, France

Manuscript received 14 February 2023; revised 11 July 2023, 30 August 2023, and 27 September 2023; accepted 16 October 2023. Date of publication 19 October 2023; date of current version 14 November 2023.

Abstract—Current sensors used in nuclear electromagnetic pulse experiments are generally shielded current transformers. Despite this shielding, calibration measurements are disturbed by common mode current interference. This letter uses a mathematical approach to limit this effect. The proposed method was applied to a test case and compared with two other techniques, including a conventional technique. The method was shown to have two benefits: to limit the influence of common mode currents and to consider the impedance mismatch effect.

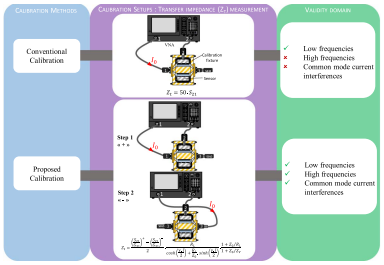

Index Terms—Sensor phenomena, common mode current, current transformer (CT), sensor phenomena, S-parameters, vector network analyzer (VNA).

I. INTRODUCTION

During nuclear electromagnetic pulse (NEMP) experiments, simulators with high-power generators, producing vertical and horizontal electric fields, are required to test equipment [1]. The resulting interference with the equipment or system placed in the simulators is measured with a wide range of sensors to probe electromagnetic fields and related variables (voltage and current) [2]. However, only current sensors are considered when observing the coupling between the NEMP wave and system cables. The current sensors are often positioned in cramped environments, such as a vehicle cabin or an aircraft cockpit, where many cables are installed. On this basis, a current sensor requires effective shielding because, once mounted on a cable, it should not measure unwanted signals from nearby cables. Moreover, current sensors need wide bandwidths and must withstand high current levels to allow for NEMP vulnerability tests [3]. Current transformers (CTs) [4] are generally one of the most suitable types of sensors for NEMP experiments. This type of sensor, shown in Fig. 1, simply consists of a transformer core with high relative permittivity and N_s turns wound, terminated by a load R. For instrumentation CTs used in NEMP studies, the transformer core and the secondary winding benefit from shield improving parasitic immunity. The CT measures the current using the principles of Faraday's law of induction. Only a variable current can, therefore, be measured, which is perfectly suited to NEMP measurements. The CT is specified by its sensitivity in the frequency domain, also called transfer impedance as defined by

$$Z_t = \frac{V_s}{I_0} \tag{1}$$

where Z_t is the ratio between V_s, the voltage measured on R terminals, and I_0, the current in the measuring conductor (primary winding). CTs are sensitive to the direction of current flow, which means that the output voltage phase can vary by 180°.

Corresponding author: Damien Gapillout (e-mail: damien.gapillout@cea.fr).
Associate Editor: Yuji Suzuki.
Digital Object Identifier 10.1109/LSENS.2023.3326102

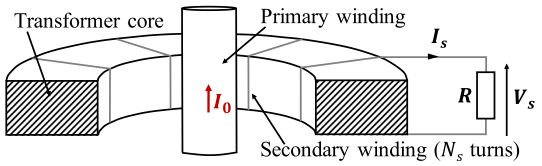

Fig. 1. Cross section of a toroidal CT clamped onto a conductor (primary winding).

CTs need to be calibrated before experiments to more reliably measure wideband pulsed currents in the time domain. This involves precisely measuring the transfer impedance. According to the conventional calibration method depicted in standards [5], [6], [7], Z_t is measured in the frequency domain using a dedicated calibration fixture (or jig) to which the sensor is clamped. However, this method does not take into account impedance mismatch between the calibration jig with the sensor and access ports. Consequently, this approach is only valid at low frequencies or for a theoretically perfectly matched system. A method was proposed to avoid these limitations in [8] and [9], except for oversized calibration fixtures. Other worthwhile techniques were developed in [10] and [11] for setups similar to the real application. Furthermore, during the frequency-domain calibration process, few phenomena appear and need to be removed or limited for accurate measurements, especially the current flowing on the outer part of the probe connector. This effect, also called common mode current, is due to the radiation produced by the current in the calibration fixture [11]. The aim of this letter is to determine, when a specific calibration fixture is used, a versatile calibration technique including mismatch effects and limiting the influence of the common mode current to benefit from more reliable calibration data.

The rest of this letter is organized as follows. Section II introduces the conventional CT calibration method. Section III describes a calibration technique based on S-parameters theory, including mismatch effect. Results are compared for a test case using the conventional technique. Section IV describes a measurement process considering

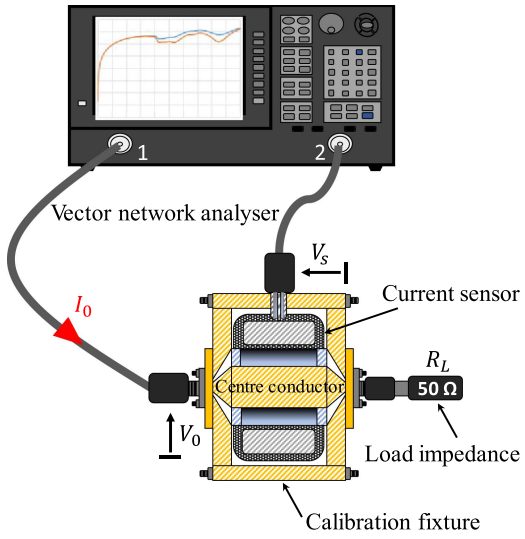

Fig. 2. Calibration setup for the conventional calibration technique with a cross section of the calibration fixture (or jig) and the sensor.

mismatches and minimizing the common mode current. This method is compared with those described in Sections II and III. Finally, Section V gives an overview of the technique used to minimize the influence of common mode currents.

II. CONVENTIONAL CALIBRATION TECHNIQUE USED FOR CTs

The measurement setup for CT calibration is based on a vector network analyzer (VNA), as illustrated in Fig. 2. Port 1 is connected to the calibration fixture to stimulate the sensor with a standard current I_0 over its bandwidth, and the second port measures V_s, the sensor's voltage response. The method, described in standards [5], [6], [7], assumes that the incoming current of the calibration fixture is the same as the outgoing current. To ensure this assumption is accurate, the geometric dimensions of the center conductor lead to a 50-Ω impedance over the calibration jig's length when the CT is clamped.

The relationship in the frequency domain between the standard current and V_0, the associated voltage is, thus, as follows:

$$I_0 = \frac{V_0}{R_L} \tag{2}$$

where R_L is a 50-Ω load impedance connected to the calibration jig's output. The transfer impedance is obtained by substituting (2) into (1)

$$Z_t = R_L \cdot \frac{V_s}{V_0}. \tag{3}$$

Finally, Z_t can be written as a forward gain coefficient S_{21} as follows:

$$Z_t = R_L \,.\, S_{21} = 50_{[\Omega]} \,.S_{21}. \tag{4}$$

This expression can be improved by referencing the jig's output current as standard current [9], [12]. However, Z_t can be better estimated with the standard current at the CT center during calibration [8]. Without considering mismatches, this expression is only valid at low frequencies. A new calibration technique is proposed below to improve the evaluation of Z_t at high frequencies in the same way as in [8] and [9] but including more mismatch effects (load impedance, VNA's load match) and for a dedicated fixture.

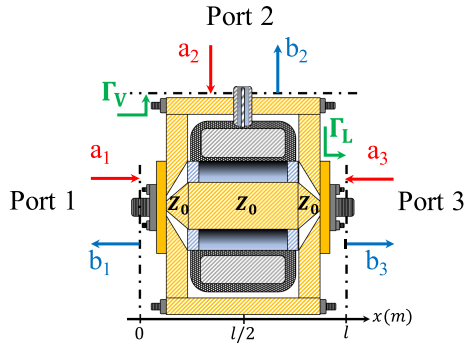

Fig. 3. Three-port network setup for the sensor clamped onto the calibration fixture. This network with the CT is equivalent to an airline of characteristic impedance Z_0 in the area between port 1 and port 3.

III. CALIBRATION TECHNIQUE INCLUDING MISMATCHES

A. Theoretical Approach

At high frequencies, setup components are generally not perfectly matched to 50 Ω. The fixture with the sensor, the load impedance, and the VNA's load match (one of the main VNA measurement error contributors [13]) must, therefore, be considered when calibrating the CT. These errors induce reflections, which are included in the calibration technique with the S-parameters theory.

The calibration fixture and the probe are defined in Fig. 3 by a three-port network where the stimuli and the responses are the a-waves and the b-waves, respectively. They are expressed as follows [14]:

$$a_i = \frac{V_i + Z_0.I_i}{2.\sqrt{Z_0}}\ ,\ b_i = \frac{V_i - Z_0.I_i}{2.\sqrt{Z_0}} \tag{5}$$

where i is the port number, V_i and I_i are the voltage and the current at port i, and $Z_0 = 50\ \Omega$ is the characteristic impedance. The method described in Section II considers a standard current I_0 at the fixture's input. A better approach is to take into account the central CT current ($x = l/2$) as a reference to enhance the transfer impedance estimate [8] since mismatches can become significant. The first step involves relating the b_3-wave to the a_1-wave using the S-parameters theory. When considering an excitation signal I_0 from port 1, the three-port network equations at ports 2 and 3 are as follows:

$$b_2 = S_{21} \,.\, a_1 + S_{22} \,.\, \Gamma_V \,.\, b_2 + S_{23} \,.\, \Gamma_L.b_3 \tag{6}$$

$$b_3 = S_{31} \,.\, a_1 + S_{32} \,.\, \Gamma_V \,.\, b_2 + S_{33} \,.\, \Gamma_L.b_3 \tag{7}$$

where Γ_V and Γ_L are the VNA's load match after VNA calibration and with load reflection coefficients such that $a_2 = \Gamma_V \,.\, b_2$ and $a_3 = \Gamma_L \,.\, b_3$.

Equation (6) can also be written as follows:

$$b_2 = \frac{S_{21} \,.\, a_1 + S_{23} \,.\, \Gamma_L \,.\, b_3}{1 - S_{22} \,.\, \Gamma_V}\ . \tag{8}$$

The relationship between b_3 and a_1 is established by inserting (8) into (7)

$$G_{31} = \frac{b_3}{a_1} = \frac{S_{31} \,.\, (1 - S_{22} \,.\, \Gamma_V) + S_{32} \,.\, S_{21} \,.\, \Gamma_V}{(1 - S_{33} \,.\, \Gamma_L) \,.\, (1 - S_{22} \,.\, \Gamma_V) - S_{32} \,.\, S_{23} \Gamma_L \,.\, \Gamma_V}. \tag{9}$$

It is now more appropriate to express a voltage gain to determine the current. a_1 and b_3 waves are related to the voltage by inserting R_L and Z_F, the load impedance, and the input impedance of the fixture

loaded by R_L, respectively, in (5)

$$a_1 = \frac{V_1 \,.\, (1 + Z_0/Z_F)}{2 \,.\, \sqrt{Z_0}} \,,\; b_3 = \frac{V_3 \,.\, (1 + Z_0/R_L)}{2 \,.\, \sqrt{Z_0}} \,. \tag{10}$$

The relationship between V_1 ($= V_0$ see Fig. 2) and V_3 is then obtained by substituting (10) into (9)

$$\frac{V_3}{V_1} = \frac{V_3}{V_0} = G_{31} \,.\, \frac{1 + Z_0/Z_F}{1 + Z_0/R_L}. \tag{11}$$

The port 3 current is deduced from (11)

$$I_3 = \frac{V_3}{R_L} = \frac{G_{31}}{R_L} \,.\, \frac{1 + Z_0/Z_F}{1 + Z_0/R_L} \,.\, V_0. \tag{12}$$

The calibration jig is similar to a coaxial airline of characteristic impedance Z_0 when the sensor is clamped (see Fig. 3), where the inner conductor is the fixture's central conductor and the outer conductor is the inner diameter of the CT. The central CT current I_{0c} is then obtained using the transmission line theory [15] assuming a perfectly centered CT and calibration fixture

$$I_{0c} = I_3 \,.\, \cosh\left(\frac{\gamma \,.\, l}{2}\right) + \frac{R_L}{Z_0} I_3 \,.\, \sinh\left(\frac{\gamma \,.\, l}{2}\right) \tag{13}$$

where l is the calibration fixture length and γ refers to the propagation constant [16] defined as

$$\gamma = \frac{1}{l} \,.\, \text{acosh}\left(\frac{1 - S_{11}^2 + S_{31}^2}{2 \,.\, S_{31}}\right). \tag{14}$$

Transfer impedance is then obtained by replacing I_0 with I_{0c} in (1) to reference the standard current at the center of the CT

$$Z_t = \frac{V_s}{I_{0c}} = \frac{V_s}{I_3 \,.\, \cosh\left(\frac{\gamma \,.\, l}{2}\right) + \frac{R_L}{Z_0} I_3 \,.\, \sinh\left(\frac{\gamma \,.\, l}{2}\right)}. \tag{15}$$

Transfer impedance has to be linked to the VNA measurands, such as S-parameters, reflection coefficients, or impedances. For this purpose, (12) is introduced into (15)

$$Z_t = \frac{1}{\left(\frac{V_0}{V_s} \,.\, G_{31} \,.\, \frac{1+Z_0/Z_F}{1+Z_0/R_L}\right) \,.\, \left(\frac{1}{R_L} \,.\, \cosh\left(\frac{\gamma \,.\, l}{2}\right) + \frac{1}{Z_0} \,.\, \sinh\left(\frac{\gamma \,.\, l}{2}\right)\right)}. \tag{16}$$

However, the V_0/V_s ratio needs also to be modified, so the VNA measurands can appear. This ratio is linked to S-parameters as shown in the following when taking real port impedances into account:

$$S_{21}\big|_{\,a_2 = \Gamma_V \,.\, b_2,\; a_3 = \Gamma_L \,.\, b_3} = \frac{V_2 \,.\, (1 + Z_0/Z_V)}{V_1 \,.\, (1 + Z_0/Z_F)} = \frac{V_s \,.\, (1 + Z_0/Z_V)}{V_0 \,.\, (1 + Z_0/Z_F)} \tag{17}$$

where Z_V refers to port 2 VNA's load match. The transfer impedance expression as a function of the VNA measurands is obtained by substituting (17) into (16)

$$Z_t = \frac{S_{21}}{G_{31}} \,.\, \frac{R_L}{\cosh\left(\frac{\gamma \,.\, l}{2}\right) + \frac{R_L}{Z_0} \,.\, \sinh\left(\frac{\gamma \,.\, l}{2}\right)} \,.\, \frac{1 + Z_0/R_L}{1 + Z_0/Z_V}. \tag{18}$$

The setup for measuring transfer impedance is similar to that shown in Fig. 1 for the conventional method, except that more acquisition steps are necessary. This is due to the consideration of full S-parameters and reflection coefficients. The relationship (18), which includes mismatch effects and with a stimulus current situated at the center of the CT, will be compared with the conventional technique for a test case in the next section.

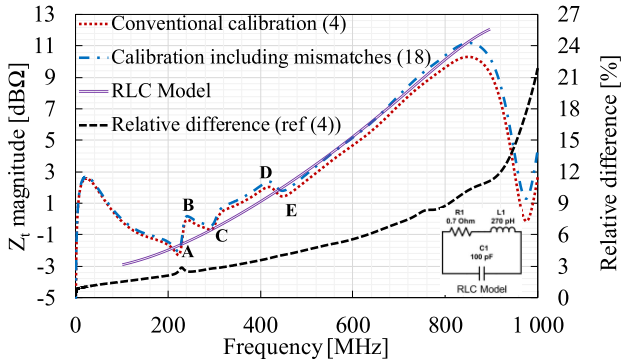

Fig. 4. Comparison of the transfer impedances obtained with the conventional technique and the technique including mismatches.

B. Comparing With the Conventional Technique

The results of technique (18) and the conventional method (4) are compared for an ETS-Lindgren 94111-2 probe. This CT operates in the (1–1000 MHz) frequency range and has a transfer impedance of 1 Ω (0 dBΩ ± 3 dB) in the frequency band (1–100 MHz). Measurements were taken for both techniques over the (100 kHz–1 GHz) frequency range with a VNA Keysight E5061B (5 Hz–3 GHz) using a SOLT calibration and a dedicated calibration fixture. The results are presented as a function of frequency in Fig. 4.

The two techniques, defined by (4) and (18), are very similar, up to 400 MHz with a relative difference of less than 5%, taking the conventional calibration as a reference. Beyond this point, the results increasingly diverge as mismatch effects are no longer negligible. The relative difference reaches 22% at 1 GHz, which is a significant value. This demonstrates the benefit of including mismatches and referencing the current at the center of the CT. In Fig. 4, the behavior of (4) and (18) fluctuates widely between curve points A and E. For this purpose, an *RLC* circuit model, the basic CT topology [17], is plotted in Fig. 4. *RLC* components ($R = 0.7$ Ω, $L = 270$ pH, $C = 100$ pF) are dimensioned to best fit measurements (4) and (18) between 200 and 840 MHz. The complete frequency response could be reproduced, but the model would be more complex and include more *RLC* components. The model based on a *RLC* cell in Fig. 4 does not have the ripples obtained in experiments between points A and E. Then, this behavior does not belong to the CT response and is therefore attributed to common mode current interference flowing on the outer part of the probe connector. The aim of Section IV is to reduce the influence of this phenomenon for Z_t.

IV. LIMITATING THE COMMON MODE CURRENT PHENOMENON WHEN CALIBRATING CTS

CTs are sensitive to the direction of the current, flowing through them, which means that the response voltage phase can be either 0° or 180°. Only parasitic elements, such as the common mode current, are insensitive to current direction. Therefore, to limit this interference, a solution based on a two-step measurement is proposed: first, a measurement is taken in a configuration identical to Fig. 3 and then the second measurement is taken by swapping ports 1 and 3 of the three-port network. The two measurements are in 180° out of phase; therefore, by calculating the difference, the common mode should be effectively removed and only the wanted signal will remain. It is essential to remember that the difference needs to be divided by two to

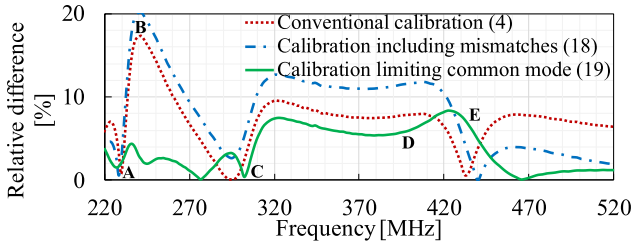

Fig. 5. Relative differences using the *RLC* model as a reference.

TABLE 1. Average Relative Difference Over the Frequency Band (220–520 MHz) Taking the *RLC* Model as a Reference

Calibration technique	Average relative difference [%]
Conventional calibration (4)	7.5
Calibration including mismatches (18)	8.8
Calibration limiting common mode (19)	3.5

avoid counting the wanted signal twice, as shown in the new expression of the transfer impedance

$$Z_t = \frac{\left(\frac{S_{21}}{G_{31}}\right)^{+} - \left(\frac{S_{21}}{G_{31}}\right)^{-}}{2} \cdot \frac{R_L}{\cosh\left(\frac{\gamma . l}{2}\right) + \frac{R_L}{Z_0} . \sinh\left(\frac{\gamma . l}{2}\right)} \cdot \frac{1 + Z_0/R_L}{1 + Z_0/Z_V} \tag{19}$$

where exponents + and − refer to Fig. 3 and to the swapped configurations, respectively. Z_t obtained using (19) for the ETS-Lindgren 94111-2 probe and previous results are plotted in relative difference as a function of the frequency in Fig. 5 using the *RLC* model as reference. These are represented in the frequency band (220–520 MHz], where the common mode shows significant impact and the model is valid (see Section III). Equation (19) has a real benefit between points A and E as it enhances the common mode rejection up to 14 percentage point (pp) especially in B, compared with the conventional method.

Moreover, the calibration technique (19) reaches an effective 3.5% average relative difference (see Table 1), which is allowing a 4 pp improvement compared with the conventional technique.

V. CONCLUSION

This letter proposes a calibration method for CTs. It covers a standard current at the center of the CT and the main mismatch effects, such as the load and calibration fixture reflections and VNA's load match. Applying this method to a test case with a dedicated calibration fixture leads to a real improvement for the transfer impedance evaluation where divergence from the conventional method reaches 22% at 1 GHz because the mismatch effects are not included. However, this method still does not prevent the common mode current from degrading the quality of the calibration process. A further improvement has, therefore, been validated and includes an additional measurement sequence to benefit from signals 180° out of phase. In areas strongly disturbed by common mode currents, the rejection is up to 14 pp (4 pp in average) for the test case when compared with other calibration techniques considered. On this basis, the proposed method can be used to more reliably determine transfer impedance for CTs because parasitic immunity is improved by the measurement technique. This enhancement proved to be very effective with the test case but would be even more worthwhile with greater mismatches and common mode currents. In the future, the impact of this calibration method must be evaluated to measure time-domain pulsed currents in the NEMP spectrum and beyond.

ACKNOWLEDGMENT

This work was supported by the France's Defence Agency.

REFERENCES

[1] M. Kreitlow, G. Schmidt, and F. Sabath, "Accreditation of a NEMP test procedure: Approach, measurement technique, uncertainty," in *Proc. IEEE Int. Symp. Electromagn. Compat.*, 2016, pp. 841–846.
[2] C. E. Baum, E. L. Breen, J. C. Giles, J. O'Nelll, and G. D. Sower, "Sensors for electromagnetic pulse measurements both inside and away from nuclear source regions," *IEEE Trans. Electromagn. Compat.*, vol. EMC-20, no. 1, pp. 22–35, Feb. 1978.
[3] L. Labarbe, "Evaluation of NEMP vulnerability on cots electronic equipments," in *Proc. Int. Conf. Electromagnetics Adv. Appl.*, 2013, pp. 102–105.
[4] S. Ziegler, R. C. Woodward, H. H.-C. Iu, and L. J. Borle, "Current sensing techniques: A review," *IEEE Sensors J.*, vol. 9, no. 4, pp. 354–376, Apr. 2009.
[5] *Requirements for the Control of Electromagnetic Interference Characteristics of Subsystems and Equipment,* NASA Standard MIL-STD-461F, Dec. 2007.
[6] "Environmental conditions and test procedures for airborne equipment," Commission Aeronaut., WA, DC, Tech. Rep. RTCA/DO-160C, 1993.
[7] *International Organization of Standardization, Road Vehicles–Component Test Methods for Electrical Disturbances From Narrowband Radiated Electromagnetic Energy—Part 4: Bulk Current Injection (BCI)*, ISO Stand. ISO 11452-4, 2005.
[8] A. R. Ruddle, "Calibration of current measurement transducers in oversized calibration fixtures," *IEEE Trans. Electromagn. Compat.*, vol. 47, no. 1, pp. 196–201, Feb. 2005.
[9] A. R. Ruddle, S. C. Pomeroy, and D. D. Ward, "Calibration of current transducers at high frequencies," *IEEE Trans. Electromagn. Compat.*, vol. 43, no. 1, pp. 100–104, Feb. 2001.
[10] G. Cerri, R. De Leo, V. M. Primiani, S. Pennesi, and P. Russo, "Wide-band characterization of current probes," *IEEE Trans. Electromagn. Compat.*, vol. 45, no. 4, pp. 616–625, Nov. 2003.
[11] D. Pommerenke, R. Chundru, and S. Chandra, "A new test setup and method for the calibration of current clamps," *IEEE Trans. Electromagn. Compat.*, vol. 47, no. 2, pp. 335–343, May 2005.
[12] H. Sekiguchi and T. Funaki, "Proposal for measurement method of transfer impedance of current probe," *IEEE Trans. Electromagn. Compat.*, vol. 56, no. 4, pp. 871–877, Aug. 2014.
[13] K. Patel and P. S. Negi, "Importance and estimation of mismatch uncertainty for RF parameters in calibration laboratories," *Int. J. Metrol. Qual. Eng.*, vol. 9, no. 4, pp. 354–376, 2012.
[14] K. Kurokawa, "Power waves and the scattering matrix," *IEEE Trans. Microw. Theory Techn.*, vol. MTT-3, no. 1, pp. 29–37, Mar. 1965.
[15] S. A. Schelkunoff, *Electromagnetic Waves*. New York, NY, USA: Van Nostrand, 1943, pp. 195–196.
[16] R. Papazyan, P. Petterson, H. Edin, R. Eriksson, and U. Gäfvert, "Extraction of high power cable characteristics from s-parameters measurements," *IEEE Trans. Dielectrics Elect. Insul.*, vol. 11, no. 3, pp. 461–470, Jun. 2004.
[17] U.-J. Kim, M.-S. Song, and R.-Y. Kim, "PCB-based current sensor design for sensing switch current of a nonmodular GaN power semiconductor," *Energies*, vol. 13, no. 19, Oct. 2020, Art. no. 5161.